Relation Between Mechanical Properties and Microstructure in CRE Type 308 Weldments

Results of creep tests and metallographic studies are analyzed to explain the improved ductility and complex behavior of a special type 308 weld metal

BY R. T. KING, J. O. STIEGLER AND G. M. GOODWIN

ABSTRACT. A shielded metal arc (SMA) type 308 stainless steel pressure vessel test weld with the controlled residual elements (CRE) boron, titanium, and phosphorus was tensile tested and creep tested at temperatures to 650 C (1200 F). Improved ductility in tests lasting several thousands of hours, compared to that of standard welds, is associated with the absence of interphase separation. Systematic variations in microstructure and mechanical properties throughout the weld and in the heat-affected zone are due to thermal and mechanical cycling during the welding process. Anisotropic deformation, that is related to local substructure and preferred crystallographic orientation, occurs.

Introduction

The use of welded pressure vessels and primary system components for power stations has been proposed for operation at temperatures at which appreciable creep deformation will occur. While neither stress nor temperature is anticipated to remain constant during service, it is not necessary to consider complex conditions to press the present understanding of the behavior of weldments to its limit. Design rules for nuclear components operating above 427 C (800 F) allow substitution of base metal properties for weld metal properties, but penalize the weld metal by allowing it to deform only half as much as base metal (Ref. 1). No explicit account is made for the stress concentrations that can occur near welds (Ref. 2).

Welds generally are heterogeneous structures. There are numerous acceptable methods for generating heat, adding filler metal, and limiting the reactions of the molten metal with its environment. Variations in the materials and welding process can affect the structure and properties of the finished weldment (Ref. 3). The complex structures of weld deposits frequently have preferred crystallographic orientations as a result of competitive growth processes during solidification (Refs. 4-7). These factors greatly influence the local subgrain and substructural characteristics of the weld metal.

In order to rationally analyze the behavior of welds under even simple conditions, the effects of these metallurgical structural features on properties should be carefully studied. At present, there is only information on basic properties for stainless steel weld metal available in the literature (Ref. 8). The current study is intended to provide further information for one weld metal of present technological interest, a type 308 stainless steel.

Thick sectons of type 304 stainless steel plate are frequently joined with type 308 stainless steel filler metal. A subclass of this type weld metal that contains 0.007% B, 0.06% Ti, and 0.04% P has been unofficially designated CRE type 308 stainless steel for the controlled residual elements which it contains. This CRE weld metal resulted from a program (Refs. 9-11) devoted to developing a type 308 stainless steel weld metal with improved ductility by tightening chemical composition limits in the range for type 308 stainless steel weld metal. Electrodes and thick section plate test welds of CRE type 308 stainless steel have been made by an industrial firm and are presently undergoing extensive tensile and creep testing.

This paper summarizes creep test results and results of metallographic studies. Large, systematic variations in mechanical properties occurred through the thickness of the test welds. The variations in properties result from systematic variations of microstructural features and, perhaps, local chemical composition variations. Another feature of the welds which complicates analyses of their behavior is anisotropy of deformation. These various aspects of weld deformation were investigated for the test welds.

Experimental Procedures

Specimen Preparation

The experimental program includes test welds made by a commercial fabricator from four batches of CRE type 308 stainless steel electrodes and two heats of type 304 stainless steel base metal. The chemical composi-

The authors are associated with the Metals and Ceramics Division, Oak Ridge National Laboratory, Oak Ridge, Tennessee.

Table 1 — Chemical Composition of Type 304 Stainless Steel Base Metal and Type 308 Stainless Steel Weld Metal Used in Study

Element	Chemical composition (wt %) of base metal from Heat 1	Heat 2	Batch 2	Chemical composition (wt %) of weld metal from Batch 4	Batch 6	Batch 9
Si	0.64	0.55	0.6	0.52	0.56	0.49
S	0.014	0.011	0.009	0.016	0.005	0.004
P	0.016	0.016	0.042	0.043	0.040	0.044
Mn	1.48	1.60	1.87	1.95	1.83	1.91
C	0.061	0.058	0.061	0.066	0.064	0.061
Cr	18.88	18.68	20.10	19.73	19.70	19.70
Ni	9.56	8.44	10.14	9.88	9.61	9.63
Mo	na[a]	na	0.24	0.25	0.07	0.24
Cb + Ta	na	na	<0.01	0.01	<0.01	<0.01
Ti	na	na	0.06	0.06	0.06	0.06
Co	na	na	0.07	0.07	0.03	0.07
Cu	na	na	0.17	0.16	0.04	0.04
B	na	na	0.007	0.007	0.007	0.007
V	na	na	0.10	0.09	0.07	0.09
N_2	na	na	0.042	0.039	0.030	0.042
Fe	na	na	bal	bal	bal	bal

(a) na = not analyzed

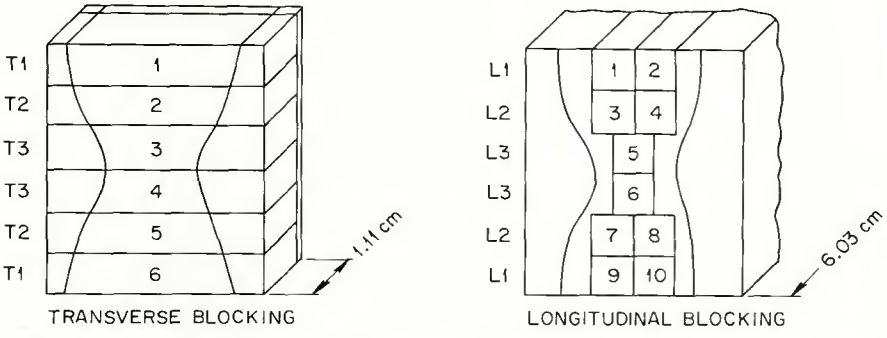

Fig. 1 — Location and orientation of standard specimens in the test weld. Hour-glass shaped region represents weld metal

tions of the deposited weld metal and base metal are given in Table 1.

The shielded metal arc (SMA) test welds were made by manually joining 15 × 20 × 6 cm (6 × 8 × 2-3/8 in.) thick sections of the stainless steel plates along the 20 cm (8 in.) length with 0.635 cm (0.25 in.) diam coated electrodes. The boron, phosphorus, and titanium content of the weld was controlled by additions of these elements to the electrode covering. The welding current and voltage were 250 A DCRP (direct current, reverse polarity) and 32 V, respectively. A double U-groove joint design (Ref. 12) was used, and constraints prevented the plates from flexing about the weld. The root pass was deposited, excess base metal was removed to assure a full penetration weld, and the grooves were filled with weld metal deposited in 35 to 40 passes. The final weld (Fig. 1) has an "hour-glass" shape and is almost symmetrical about the midplane of the plate. It is two passes wide everywhere except at the root.

The mechanical properties testing program involved two types of as-welded specimens, a standard specimen with a 0.635 cm diam by 3.175 cm (0.25 in. diam by 1.25 in.) long gage section and a "buttonhead" specimen with a 0.317 cm diam by 2.86 cm (0.125 in. diam by 1.25 in.) long gage section. Standard specimens were cut from the weld in both longitudinal and transverse directions as shown in Fig. 1. The results justify grouping the specimens according to distance from the nearest plate surface regardless of the side of the midplane from which they came. Thus, specimens of the L1, L2, and L3 types and specimens of the T1, T2, and T3 types all have center lines '.5, 1.4, and 2.4 ± 0.2 cm (0.19, 0.56, and 0.94 ± 0.08 in.) below the nearest plate surfaces, respectively. The buttonhead specimens were longitudinally oriented at the same distances beneath the plate surface, but they were cut from a seven specimen (across) by six specimen (high) square grid. Buttonhead specimens were made that contained either all-weld-metal, all-base-metal, or part-weld-metal (fusion line) specimens.

Testing Procedures

Both tensile and creep tests were run on the standard specimens. Nearly all of the standard creep and tensile specimens were fitted with averaging extensometers. The details of testing procedures are given elsewhere (Ref. 13). Tensile tests were performed at a nominal strain rate of 0.004 min^{-1} (these Instron tests were not strain-rate controlled) at temperatures between room temperature and 649 C (1200 F). Creep tests were performed at 482, 565, 593, and 649 C (900, 1050, 1100, and 1200 F).

Most buttonhead specimens were tested at 593 C (1100 F) using a non-averaging extensometer fitted with a dial gage. Most of the specimens were tested under a nominal uniaxial stress of 241 MPa (35,000 psi).

Microscopy Procedures

Optical and electron microscopy were used to study as-received wafers from selected regions of the weld and base metals. Sections were cut parallel and perpendicular to the welding direction. These wafers were thinned electrolytically and examined by transmission electron microscopy to determine any variation in the microstructure. Quantitative measurements of dislocation and precipitate densities were made using stereo techniques to determine foil thickness and dislocation densities in three dimensions. The correction for invisible dislocations was made by assuming all Burgers vectors to be equally probable, an assumption that was verified in some regions by examining two or more reflections.

The fracture surfaces of selected specimens were examined with a scanning electron microscope. The gage sections were then cut to show three orthogonal surfaces in the broken specimen, two parallel and one normal to the load axis. The sections were mounted, polished, etched, and examined metallographically.

Results

Mechanical Properties

In tensile tests at temperatures of 25, 482, and 592 C (77, 900, and 1100 F), there were no consistent differences in properties related to the batch of electrodes or the heats of base metal which were joined. A salient feature is the variation of properties which occurs through the thickness of the weld. The weld metal from the L1 position near the surface always has yield strengths between 34.5 and 103 MPa (5,000 and 15,000 psi) lower than weld metal from the L3 position near the center of the weld. Typical results obtained at 482 C (900 F) that indicate the amount of scatter normally encountered in tensile tests are shown in Fig. 2. No significant variations of ultimate tensile strength with location were observed. Specimens from

the L3 position near the weld center had significantly lower uniform and total strains than specimens from the L1 position near the weld surface, but the uniform and total strains always exceeded 3 and 20%, respectively (Fig. 3).

A few transverse tensile specimens were also tested. They tended to exhibit higher than average strength (Fig. 2).

Because creep tests were performed at several temperatures, it is convenient to represent the creep data by a time-temperature parameter method. The Larson-Miller parameter is used here because of its relative simplicity and widespread acceptance. The Larson-Miller representation of creep data has the form (Ref. 14):

$$\log_{10}\sigma = f\,[T(c + \log_{10} t)]\ ,$$

where T is temperature (R) (1 K = 1.8 R), σ is applied stress (Pa), and the constant, c, is arbitrarity set equal to 20. The time, t, refers to specific identifiable times in a creep test: time to 1% strain ($t_{1\text{-}0}$) is shown as an example of relatively small strain data. These time data are presented in Figs. 4 and 5, respectively, together with ASME Code Case 1331-6 average values for type 304 stainless steel (Ref. 2). These times were obtained manually from the strain-time graphs. Throughout the graphical presentations, the specimen location for each datum is identified.

The differences in behavior of L1, L2, and L3 specimens are readily distinguished at small strains for $t_{1\text{-}0}$ (Fig. 4). This observation also is true to the time-to-rupture plot (Fig. 5). For comparison, the approximate limits for stress to cause rupture for type 304 stainless steel base metal are included (Ref. 15). Different limits are shown for different testing temperatures because the limits were originally derived on other bases than the Larson-Miller parameter. The confidence limits shown are ±1.645 st'd deviations. The total strain is plotted versus the log of the rupture time in Fig. 6. Again, the identity of specimen locations is shown for all tests.

Comparisons of the strain-time behavior of longitudinal and transverse standard specimens at 593 C (1100 F) for 227.5 MPa (33,000 psi) stress are shown in Fig. 7. Direct comparisons may be made between the L1 and T1 specimens, and the L3 and T3 specimens. The deformation resistance of the weld metal is different in different directions, even considering the presence of base metal from the heat-affected zone in the transverse specimens; transverse specimens are significantly stronger than longitudinal all-weld-metal specimens under these test conditions.

The total elongations and rupture times for the buttonhead specimens tested at 593 C (1100 F) and 241 MPa (35,000 psi) are mapped in Fig. 8. Failure times for base metal distant from the fusion line range between 100 and 700 h, and strains all exceed 12%. Base metal specimens from the heat-affected zone near the fusion line failed in times between 250 and 1200 h at strains on the order of 10% or less. All-weld-metal

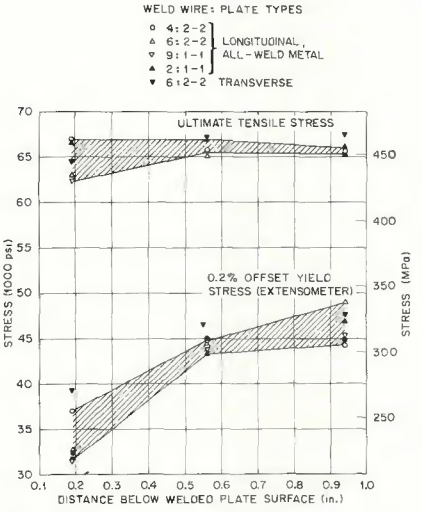

Fig. 2 — Tensile properties of CRE type 308 stainless steel weld metal at 482 C and 0.004/min strain rate. Different batches of welding electrodes and heats of base metal are identified separately (See Table 1)

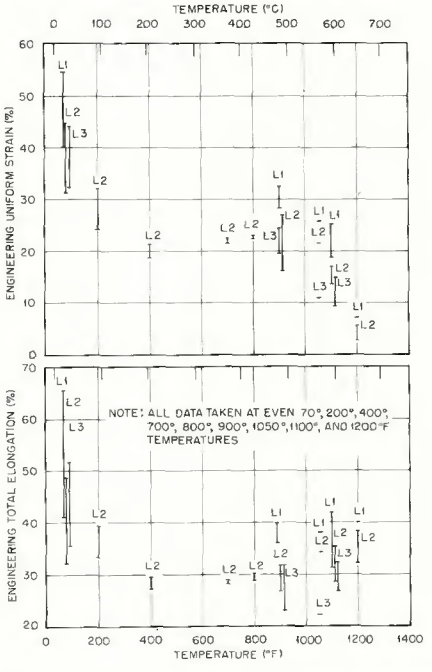

Fig. 3 — Tensile strain properties of type 308 CRE longitudinal all-weld-metal specimens tested at 0.004/min strain rate

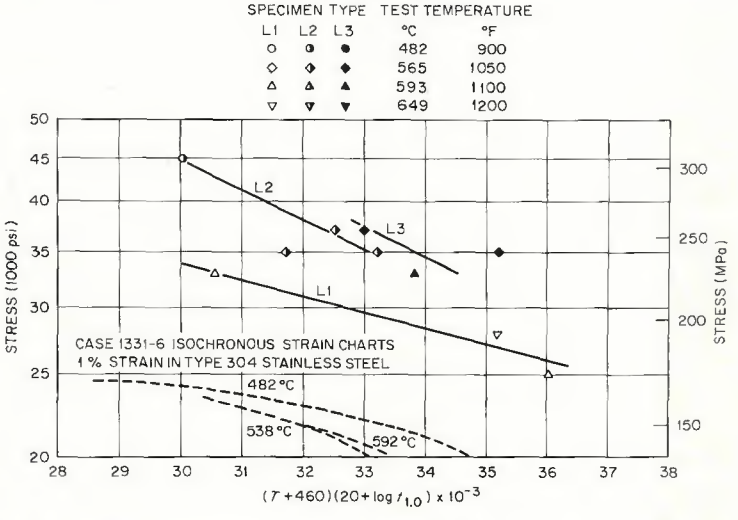

Fig. 4 — Larson-Miller parameter for time to 1.0% strain in CRE type 308 stainless steel weld metal

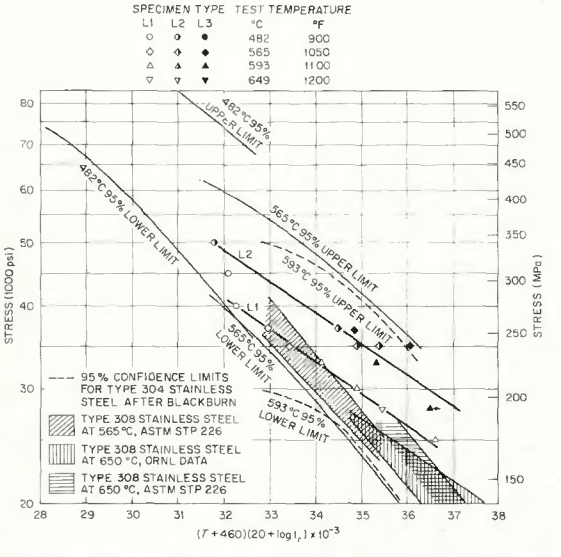

Fig. 5 — Rupture times of CRE type 308 stainless steel weld metal compared with standard weld metal and Type 304 stainless steel base metal, represented by the Larson-Miller parameter

specimens failed in less than 100 h at strains greater than 18%. The properties of specimens containing the fusion line depend upon the fraction of the gage section that is comprised of weld metal.

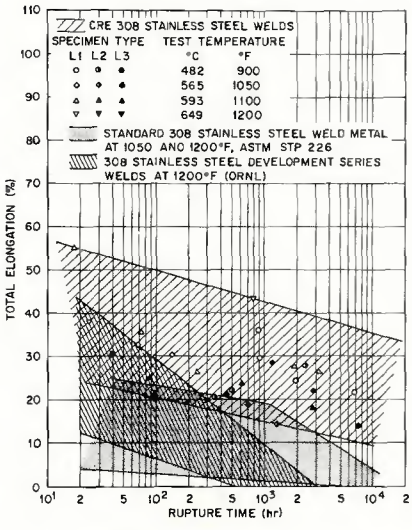

Fig. 6 — Ductility in creep-rupture tests of type 308 stainless steel welds

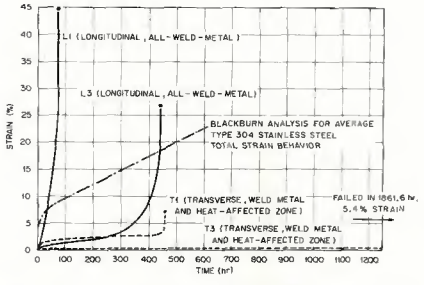

Fig. 7 — Comparison of longitudinal and transverse creep specimens of CRE type 308 stainless steel weld metal at 593 C, 228 MPa (33,000 psi). Failure did not occur in weld metal in transverse specimens

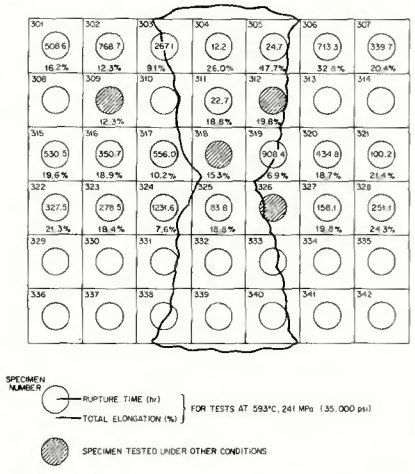

Fig. 8 — Map of rupture times and total elongations for CRE type 308 stainless steel weld metal, Type 304 stainless steel base metal. Hourglass region is weld metal

Microscopy Results

The microstructures of the weld were typical of type 308 stainless steel weld metal containing 5 to 8% ferrite (Ref. 3). A continuous austenite matrix separated long, narrow, ferrite regions that were distributed in a cellular dendritic pattern. The substructural boundaries visible in Fig. 9(a) are apparently aligned nearly parallel to the solidification direction, and they separate columnar austenite subgrains which appear to grow epitaxially from the base metal into the weld metal and across interpass boundaries in many cases. The ferrite distribution and orientation of the long axes of the grains vary with location within the weld, depending on the solidification growth direction (which, in turn, is controlled by the shape of the molten weld metal puddle during welding) (Ref. 5).

Transmission electron microscopy at 650 kV revealed the systematic variation in the microstructure of the weld metal, shown in Fig. 9(b) and (c). The results are also summarized in Table 2. The austenite phase of weld metal contained in L1 or T1 (surface) specimens had about 1×10^{10} straight dislocations/cm² with a poorly developed cell structure; the austenite-ferrite interfaces in this region were free of visible precipitate particles, Fig. 9(b). Near the center of the weld in a region contained by L3 and T3 specimens, there were about 2.8×10^{10} dislocations/cm² arranged in a well-defined cell structure together with some 5.5×10^{15} loops/cm³. The austenite-ferrite boundaries are nearly covered with $M_{23}C_6$ precipitates. In the center region, the precipitates are massive and their crystallographic orientation is parallel to that of the austenite matrix, Fig. 9(c). At the intermediate L2 and T2 locations, there were about 2×10^{10} dislocations/cm² in the austenite, and the

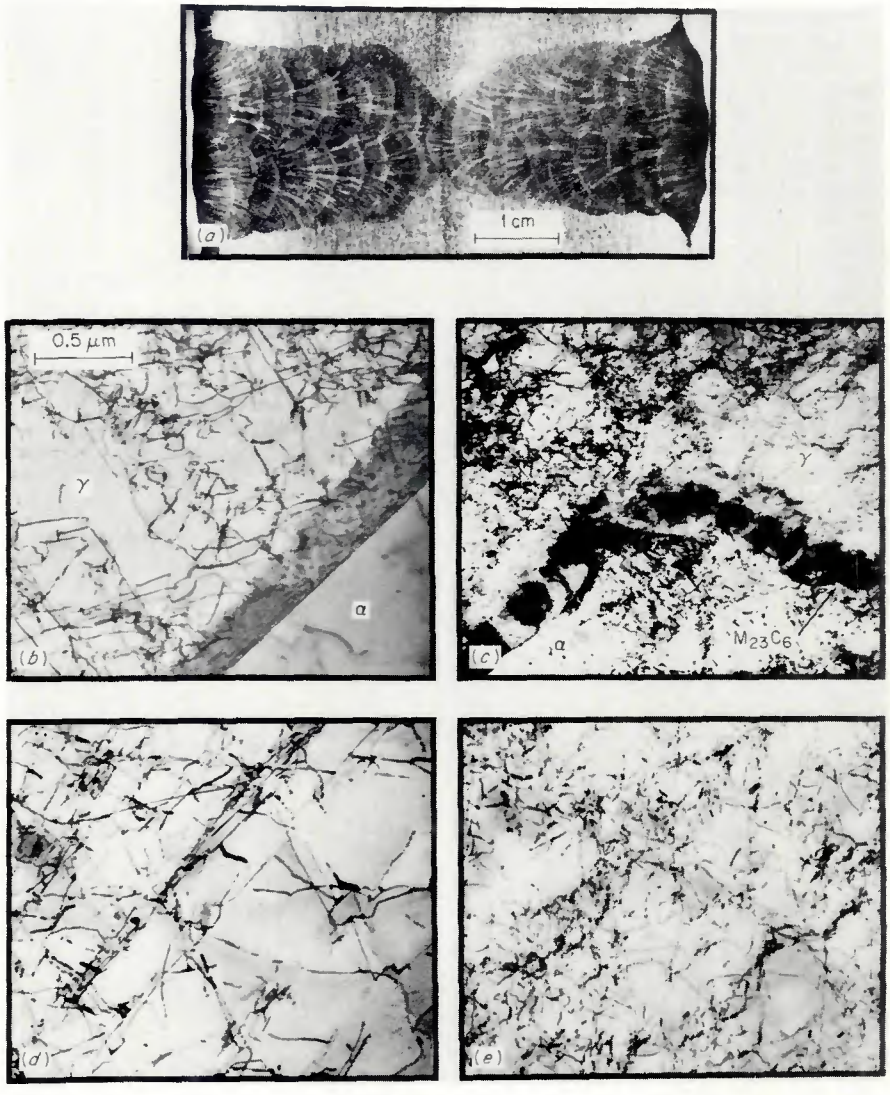

Fig. 9 — As-welded microstructure of CRE type 308 stainless steel weldment. (a) Macrostructure; (b) weld metal contained in L1 type specimen; (c) weld metal contained in L3 type specimen; (d) base metal 1.5 cm below surface, 1.0 cm from fusion line; (e) base metal 1.5 cm below surface, 0.1 cm from fusion line

interphase boundaries were decorated with a platelike $M_{23}C_6$ precipitate. The dislocation density in ferrite was generally a factor of 2 to 10 lower than in the austenite, but it tended to be highest locally where ferrite widths were small.

The structures of the heat-affected zone and as-received type 304 stainless steel base metal 1.5 cm beneath the weld surface are shown in Fig. 9(d) and (e), respectively. There was no discontinuity in the dislocation structure at the fusion line. At a distance of 0.1 cm from the fusion line, a density of 1.6×10^{10} dislocations/cm^2 existed as compared with a density of 0.5×10^{10} dislocations/cm^2 at a distance of 1.0 cm from the fusion line. Near the fusion line, dislocation tangles and cell structures resembled those in the austenitic weld metal at a similar distance from the surface. At a distance of 1 cm from the fusion line, straight dislocations typical of a light, low temperature deformation were found. There were no observable precipitates formed in the base metal during welding. These observations are also summarized in Table 2.

The microstructures of tested all-weld-metal creep specimens all show general elongation parallel to the tensile axis. Two reactions were observed in the weld metal whose rates depend on time, temperature, and perhaps strain: the cellular dendritically distributed ferrite in the weld metal transforms to sigma phase during testing, and the $M_{23}C_6$ carbide precipitates dissolve. The transformation to sigma phase has been observed by optical metallography and verified by electron diffraction techniques. No dislocations were ever found in the sigma phase, which is relatively hard.

Surprisingly, internal cracks were not found in the tested CRE weld metal, even after creep tests lasting several thousands of hours at 593 C (1100 F). Failures occurred by shear and ductile tearing, as evidenced by the dimpled fracture surfaces (Fig. 10). Occasional ledges on the fracture surfaces can be attributed to diversion of the fracture path along weak interphase boundaries, but the predominant mode of fracture propagation in creep tests was not strongly influenced by substructural cracking.

Table 2 — Defect Statistics in CRE Type 308 Stainless Steel Test Welds, As-Welded Condition

Region	Depth below surface, cm	Phase	Dislocation density, cm/cm^3	Loop density, loops/cm^3	Matrix precipitate density, particles per cm^3	Austenite-ferrite interface, $M_{23}C_6$ precipitates
Weld	0.25	Austenite	1.0×10^{10}	P[a]	O[b]	O
Weld	1.5	Austenite	2.05	P	O	P[c]
Weld	3.0	Austenite	2.8	5.5×10^{15}	O	P[d]
Weld	1.5	Ferrite	0.9	O	O	
HAZ[e]	1.5	Austenite	1.6	P	O	
HAZ[f]	1.5	Austenite	0.5	P	O	

(a) P = present but not measured
(b) O = absent
(c) Plate-like particles
(d) Massive particles
(e) 0.1 cm from fusion line
(f) 1.0 cm from fusion line

Discussion

Relation Between Properties and Structure in the Weldment

Events which occur during welding control the local properties and microstructure of the as-deposited weld metal and the heat-affected zone. Metal deposited before the last pass experiences a complex thermomechanical history when later weld passes are deposited. Solidification shrinkage stresses and thermal stresses (Refs. 16, 17) contribute to relatively heavy deformation of the initial passes, resulting in the high observed dislocation and loop density near the center of the weld. Precipitation of $M_{23}C_6$ carbides at elevated temperatures is a well known phenomenon in austenitic steels that is sensitive to a number of metallurgical variables, including prior thermal and mechanical treatments (Ref. 18). The systematic variations of dislocation structure and carbide precipitate structure and density through the thickness of the weld (Table 2) are a result of the greater number of thermal and mechanical cycles experienced in the initial passes than in the surface weld passes.

The variation of yield stress with location in the weld (Fig. 3) has been semiquantitatively related to the local density of dislocations in the austenite (Ref. 19), although other factors such as local chemical composition also must affect the yield stress to some degree. The increment in yield stress due to an array of dislocations is proportional to the square root of dislocation density. Although there are no adequate theories relating creep behavior to initial microstructure, the difference in stress required to cause 1.0% strain in the L1, L2, and L3 specimens of CRE weld metal (Fig. 4) can be tentatively ascribed to the observed systematic microstructural variations. In essence, the heavily deformed as-deposited weld metal from the center of the weld is stronger at small strains than weld metal near the surface. This observation is in agreement with the measured yield strength variation. Effects due to second phases and local chemical composition variations are also recognized to have possible importance, and these variables are now being investigated in greater detail.

Creep behavior variations with location in the weld at small strains do persist at larger strains or longer test times. About 20% higher stresses are required to cause failure for L3 specimens at a given time-temperature parameter value than are required for L1 specimens.

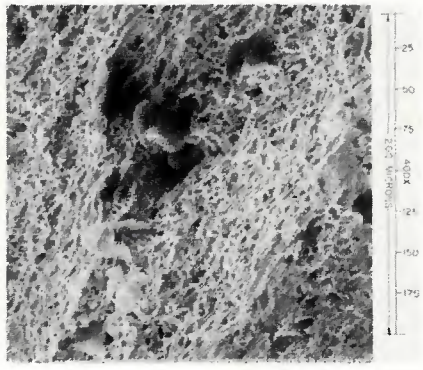

Fig. 10 — Scanning electron micrograph of CRE type 308 stainless steel weld metal. Creep to failure in 2394.6 h at 482 C. Some oxide scale and embedded inclusions are visible on the fracture surface

The lowest observed total creep strain (Fig. 6) for any all-weld-metal creep specimen of CRE type 308 stainless steel is 13%. All of the total strain data are contained in a single scatter band when plotted versus rupture time. The band shows decreasing ductility with increasing time to rupture. There is some tendency for longitudinal, all-weld-metal specimens to be more ductile than specimens from the center of the weld (Fig. 6).

Anisotropy of plastic deformation of the weld metal is evident in both the tensile and creep data. The transverse weld metal specimens are consistently stronger than the longitudinal specimens. They are oriented differently with respect to the local solidification substructure. Other work (Ref. 19) has demonstrated that CRE weld metal deforms relatively easily in the direction parallel to the local substructure, leading to nonuniform diametral reductions similar to those reported for other steel weld deposits (Ref. 20). At least two interrelated factors influence anisotropic deformation, the observed preferred

crystallographic orientation of the weld metal (Refs. 4-7) and the local substructural orientation. Preliminary indications of preferred orientations have been found experimentally by x-ray techniques for CRE type 308 stainless steel weld metal (Ref. 21). The substructural orientation is usually parallel to local orientation of the elongated ferrite phase, the longest mean free path between subgrain boundaries, and, in regions where M C_6 precipitates occur, the longest mean free path between walls of hard precipitate particles lying on interphase boundaries. During creep tests the original ferrite phase transforms to sigma phase, and these hard precipitates should make deformation more difficult in all directions except parallel to the local substructure. Any or all of these factors may contribute to anisotropic deformation under given testing conditions, but the relative importance of each is not yet ascertained.

The type of thermal and stress cycling which contributed to the variations of structure through the as-deposited weld metal is responsible for the variation in properties and microstructure of the nearby type 304 stainless steel base metal. The heat-affected zone of the base metal in the test welds experienced a series of complex thermomechanical cycles during the deposition of successive weld passes which had little observable effect on the microstructure except to increase the local dislocation density near the fusion line, Fig. 9(d) and (e). However, this cycling may have influenced the stress aging (Ref. 22) that can occur at low stresses or dynamic strain aging processes during deformation (Ref. 23), both of which affect the properties of austenitic steels. The net effect on properties in the heat-affected zone was to increase the rupture time while decreasing the total elongation relative to the as-received base metal. Note that buttonhead specimens which were part weld metal and part heat-affected base metal can exhibit a wide range of properties, depending upon the proportions of the ductile, relatively weak weld metal and the less ductile but relatively strong heat-affected zone base metal in the gage section.

Relation Between Metallographic Features and Ductility of Weld Metals

The creep rupture strengths of the CRE type 308 stainless steel weld specimens of the L1, L2, and L3 types tend to be similar to or higher than those reported for standard type 308 stainless steel weld metal (Refs. 8, 10). However, the ductility of the CRE weld metal is clearly superior to values reported for standard weld metal from the same sources. With the exception of one datum for standard weld metal, all the elongations for standard weld metal lie within an envelope whose upper limit is near the lower limit of the ductility scatter band of CRE weld metal. An extrapolation of the envelope approaches zero total strains for standard weld metal at about 10,000 h rupture times. On the other hand, although the scatter band for CRE weld metal indicates decreasing rupture strains for long rupture times, no strain less than 13% has been recorded for tests lasting up to 7550 h, and the ductility scatter band for the CRE all-weld-metal specimen does not extrapolate to zero in 300,000 h.

The differences in ductility between the standard and CRE weld metal can be related to differences in the fracture mode. For long time creep ruptures at 649 C (1200 F), the fracture in standard weld metal frequently initiates at original austenite-ferrite boundaries and the final fracture links thse internal cracks (Refs. 5, 9). The transformation of ferrite to sigma phase and dissolution of carbides occur under these test conditions (Ref. 24) and at other temperatures with different reaction kinetics (Ref. 18), providing a variety of interphase boundaries to serve as fracture paths that parallel the original austenite-ferrite boundaries. Extensive sigma phase-austenite boundary separations that initiate fracture and result in the low ductility fracture in standard type 308 stainless steel weld metal have been observed (Ref. 24).

Conversely, the interphase boundaries in CRE type 308 stainless steel weld metal do not separate internally during creep tests. The predominantly shear fracture surfaces occasionally are diverted along substructural features, but no metallographic or electron microscopy evidence for fracture initiated by internal cracking has been found. All of the types of interphase boundaries found in standard weld metal also exist in the CRE weld metal. The reason for this difference in behavior is not known (Ref. 24).

Implications for Detailed Analyses of Weldments

A great deal of effort is presently being directed toward understanding the behavior of weldments in greater detail. Numerical finite element analyses of the stress-strain state during welding (Ref. 25) and of weldments during deformation (Refs. 26-30) have shown nonuniformity of stress and strain distributions in weldments, even when various regions of weldments are treated as homogeneous, isotropic media. Quite clearly, an accurate description of the actual weldment investigated here would require continuously varying mechanical properties throughout the weld metal and heat-affected region, and the inclusion of anisotropic deformation characteristics for the weld metal with a point-to-point variation in the orientation of the principal axes of anisotropy. Design considerations based on the behavior of the most highly stressed or strained element of the weld metal or weldment might then be developed.

Summary

The creep and tensile properties of a shielded metal arc, multipass, type 308 stainless steel, pressure vessel test weld have been investigated at temperatures to 649 C (1200 F). The particular weld contained controlled amounts of the residual elements B (0.007%), Ti (0.06%), and P (0.04%) and is designated CRE (controlled residual element). Results of the investigation showed the following for as-deposited weld metal and heat-affected zones:

1. Systematic variations in microstructure occur through the thickness of the weld. In the initial passes at the center of the weld, dislocation densities are highest, dislocation loops form, cell structures form, and $M_{23}C_6$ carbides precipitate on austenite-ferrite interfaces as a result of numerous thermal and mechanical cycles experienced during welding. The carbide precipitate density, loop density, and dislocation density decrease gradually toward the surface of the weld where less thermal and mechanical cycling occur. Near the surface proper, few dislocation loops and no precipitates are present and the dislocation density is about a factor of 2.8 lower than near the center of the weld. The dislocations near the surface are, generally, straight and only a hint of crude cell structure occurs.

2. Systematic variations in creep properties at small and large strains and in tensile properties are at least partly attributable to these microstructural variations. Weld metal from initial passes is stronger than weld metal in the final passes.

3. Dislocation densities in base metal from the heat-affected zone increase near the fusion line. Due to the complex thermal and mechanical cycling, type 304 stainless steel base metal from near the fusion line is stronger but less ductile than base metal unaffected by welding.

4. Anisotropic deformation influenced by the local substructural orientation and/or preferred crystallographic orientation occurs; since these orientations vary throughout the weld, the principal axes of anisot-

ropy also vary with location. Transverse specimens are stronger in creep than longitudinal, all-weld-metal specimens under the test conditions explored.

5. Internal cracks did not develop at interphase boundaries of CRE weld metal. The ductility of CRE weld metal is superior to published data for standard type 308 stainless steel weld metal that does crack internally at interphase boundaries.

Acknowledgements

The authors wish to thank E. Bolling, J. K. Alley, and S. W. Cook for their diligent efforts on the experimental work. Gratitude is also expressed to E. W. Pickering, Jr., J. F. Turner, and C. T. Ward of Combustion Engineering, Chattanooga, for their efforts in preparing the test welds. The encouragement of and fruitful discussions with P. Patriarca, J. R. Weir, Jr., W. R. Martin, H. E. McCoy, G. M. Slaughter, N. C. Cole, D. A. Canonico, and R. G. Berggren are gratefully acknowledged.

The research work was sponsored by the U.S. Atomic Energy Commission under contract with the Union Carbide Corporation.

References

1. Case 1331-6, *Interpretations of ASME Boiler and Pressure Vessel Code,* (American Society of Mechanical Engineers, New York) 1972.

2. Walters, D. J., Rowley, T., and Elder, W. J., "The Creep Assessment of Butt Welded Pipes and Tubes," paper presented at International Conference on Welding Research Related to Power Plant, Sept. 17-21, 1972, Central Electricity Generating Board Marchwood Engineering Laboratories, England.

3. Goodwin, G. M., Cole, N. C., and Slaughter, G. M., "A Study of Ferrite Morphology in Austenitic Stainless Steel Weldments," *Weld. J. (Miami)* September 1972 *51*(9), 425s-429s.

4. Savage, W. F., Lundin, C. D., and Aronson, A. H., "Weld Metal Solidification Mechanics," *Weld. J. (Miami)* April 1965 *44*(4), 175s-181s.

5. Savage, W. F., and Aronson, A. H., "Preferred Orientation in the Weld Fusion Zone," *Weld. J. (Miami)* February 1966 *45*(2), 85s-89s.

6. Aronson, A. H., "Growth Mechanisms in the Weld Fusion Zone," January 1965, Thesis, Rensselaer Polytechnic Institute, Troy, New York.

7. Chase, T. F., "An Investigation of the Solidification Mechanics of Fusion Welds in Face-Centered Cubic Metals," January 1967, Thesis, Rensselaer Polytechnic Institute, Troy, New York.

8. Voorhees, H. R., and Freeman, J. W., "The Elevated-Temperature Properties of Weld-Deposited Metal and Weldments," ASTM Spec. Tech. Publ. 226, American Society for Testing and Materials, Philadelphia, 1958.

9. Binkley, N. C., Goodwin, G. M., and Harman, D. G., "Effects of Electrode Coating on Elevated-Temperature Properties of Austenitic Stainless Steel Weld Metal," *Weld J. (Miami)* July 1973 *52*(7), 306s-311s.

10. Binkley, N. C., Berggren, R. G., and Goodwin, G. M., "Effects of Slight Compositional Variation on Type E308 Electrode Deposits," to be published in *Welding Journal (Miami).*

11. Slaughter, G. M., "Joining of Structural Materials," *Metals and Ceramics Div. Annu. Progr. Rep. June 30, 1972,* ORNL-4820, pp. 72-75.

12. "Fundamentals of Welding," p. 1.46 in Section 1 of the *Welding Handbook 1968,* 6th edition (American Welding Society, New York).

13. King. R. T., Stiegler, J. O., and Goodwin, G. M., "Creep Properties of a Type 308 Stainless Steel Pressure Vessel Weld with Controlled Residual Elements," paper presented at International Conference on Creep and Fatigue in Elevated-Temperature Environments, Joint ASTM-ASME-IME Meeting, Philadelphia, Pa., Sept. 23-28, 1973, to be published in proceedings.

14. Roberts, D. I., and Sterling, S. A., "A Parametric Method for the Development of Isochronous Stress-Strain Curves," pp. 1-14 in *The Generation of Isochronous Stress-Strain Curves,* 1972, ed. by A. O. Schaefer (American Society of Mechanical Engineers, New York).

15. Blackburn, L. D., "Isochronous Stress-Strain Curves for Austenitic Stainless Steels," p. 16 in *The Generation of Isochronous Stress-Strain Curves,* 1972, ed. by A. O. Schaefer (American Society of Mechanical Engineers, New York).

16. Williams, N. T., Smith, C. F., and Toft, L. H., "Stresses and Strain in Thick Austenitic Steel Plates During Welding," pp. 143-148 in *Proceedings of the Second Commonwealth Welding Conference, April 26-May 16, 1965,* (Institute of Welding, London).

17. Cepolina, A. G., and Cananico, D. A., "The Measurement of Residual Stresses," *Weld. J. (Miami)* January 1971 *50*(1), 31s-38s.

18. Weiss, B., and Stickler, R., "Phase Instabilities During High Temperature Exposure of 316 Austenitic Stainless Steel," *Met. Trans.* April 1973 *3,* 851-866.

19. King, R. T., Stiegler, J. O., and Goodwin, G. M., "Properties of Thick Type 308 Stainless Steel Welds with Controlled Residual Elements," submitted to *Transactions of the American Institute of Mining and Metallurgical Engineers.*

20. Heuschkel, J., "Anisotrophy and Weldability," *Weld. J. (Miami)* March 1971 *50*(3), 110s-126s.

21. Bernal, J., and Vandermeer, R. A., private communication.

22. Harrington, R. H., "Stress-Aging and Its Effects on the Standard Tensile Properties of Some Stainless Steels," *Trans. ASM* 1965 *58,* 119-141.

23. Garafalo, F., Von Gemmingen, F., and Domis, W. R., "The Creep Behavior of an Austenitic Stainless Steel Effected by Carbides Precipitated on Dislocations," *Trans. ASM* 1961 *54,* 430-444.

24. Stiegler, J. O., King, R. T., and Goodwin, G. M., "Effect of Residual Elements on Fracture of Type 308 Stainless Steel Weld Metal," paper presented at Winter 1973 ASTM Meeting, Detroit, Mich., Nov. 12-15, 1973, to be published in proceedings.

25. Hibbih, H. D., and Marcal, P. V., "A Numerical, Thermo-Mechanical Model for the Welding and Subsequent Loading of a Fabricated Structure, to be published.

26. Chan, S. K., Manjoine, M. J., and Visser, C., "Analysis of Stresses in Pressurized Pipe in the Creep Range," ASME 71-PVP-66 (American Society of Mechanical Engineers, New York) 1971.

27. Walter, D. J., and Cockroft, R. D. H., "A Stress Analysis and Failure Criteria for High Temperature Butt Welds," paper presented at the International Institute of Welding Colloquium on Creep Behavior of Welds in Boilers, Pressure Vessels, and Pipelines, Toronto, 1972.

28. Townley, C. H. A., Goodall, I. W., and Lewis, D. J., "Design Criteria for Welded Pressure Parts," paper presented at International Conference on Welding Research Related to Power Plant, Sept. 17-21, 1972, Central Electricity Generating Board Marchwood Laboratories, England.

29. Hardy, A. K., Goodall, I. W., and Rowley, T., "Design and Operational Aspects of Steam Pipe Transition Joints," International Conference on Welding Research Related to Power Plant, Sept. 17-21, 1972, Central Electricity Generating Board Marchwood Laboratories, England.

30. Chubb, E., Fidler, R., and Wallace, D., "Development and Relaxation of Welding Stresses," International Conference on Welding Research Related to Power Plant, Sept. 17-21, 1972, Central Electricity Generating Board Marchwood Laboratories, England.